Progress In Electromagnetics Research, PIER 66, 287–299, 2006

ANALYSIS OF A LOSSY MICRORING USING THE GENERALIZED MULTIPOLE TECHNIQUE

N. Talebi and M. Shahabadi

Photonic Research Laboratory
School of Electrical and Computer Engineering
University of Tehran
North Kargar Ave., Tehran, Iran

C. Hafner

Laboratory for Electromagnetic Fields and Microwave Electronics
ETH Zurich
Gloriastrasse 35, CH-8092 Zurich, Switzerland

Abstract—In this work, the performance of a microring add-drop filter is investigated using the generalized multipole technique. The complete scattering parameters of the structure are computed using an efficient port solver based on the generalized multipole technique, which avoids spurious reflections at the terminations. The scattering parameters of a number of structures are calculated and compared with those obtained using the FDTD and coupled-mode theory methods. The generalized multipole method can advantageously take dielectric losses of the microring into account. Moreover, the total power loss including radiation and the dielectric losses is computed for a microring add-drop filter, for the first time.

1. INTRODUCTION

Optical ring resonators are used in many applications such as channel dropping filters, dispersion compensators, optical switches, and lasers [1–6]. These resonators are mostly characterized by parameters such as free spectral range (FSR), quality factor (Q), insertion loss (IL), and crosstalk (XT). A typical two-dimensional microring add-drop filter is shown in Figure 1. Recently high-index-contrast ring resonators attracted much attention, because they allow one to fabricate very small ring resonators with low radiation loss. The realization of such

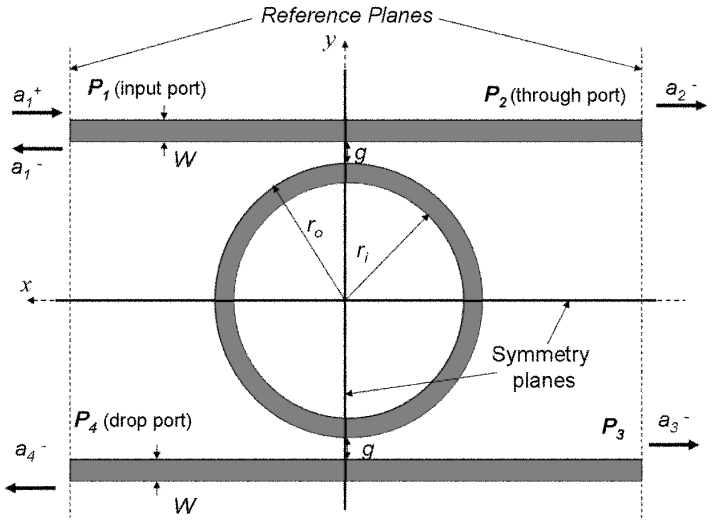

Figure 1. A microring add/drop filter.

structures requires nanofabrication techniques for rings with radii as small as $1\,\mu$m [7].

So far these resonators have been investigated using the beam propagation method (BPM), the finite deference time domain (FDTD) method, and coupled mode theory (CMT). Among these methods, FDTD is most frequently applied because of its flexibility in the analysis of complex structures. However, its precision is limited because it is based on a second order scheme, because absorbing boundary conditions are required to truncate the surrounding space and the waveguides [8, 9], and because of the staircase discretization of the curvilinear structures. In addition to these factors, the excitation of the structure with fields other than the modal fields of the connecting waveguides can lead to difficulties regarding the size of the simulation domain and also the simulation time. Finally, Fourier transform is required for obtaining the frequency response.

The generalized multipole technique (GMT) is a frequency domain method that is very flexible for isotropic and piecewise linear materials. This method has been successfully applied to complicated structures such as photonic-crystal components [10, 11]. In contrast to FDTD, it only requires the discretization of the boundaries, which exhibits therefore no problems with open space and provides exponential convergence for the smooth geometry of the ring resonators. To obtain the exact modal scattering parameters of the microring, we benefit from a port solver based on the generalized multipole technique

which has been already applied to the analysis of certain waveguide discontinuities. This method avoids the spurious reflections which naturally occur in other methods due to the impedance mismatch at waveguide terminations. We also take the four-fold symmetry of the microring add-drop filter into account, which results in better accuracy and reduced computation time. The influence of the dielectric loss on the transmittance behavior of the ring resonator add-drop filter, such as IL and Q will also be discussed. Since GMT is a frequency domain method, it can easily take the dielectric loss into account in any data format such as experimental diagrams or Drude or Lorentz model. It will be shown that dielectric losses can deteriorate the performance of these resonators, and even suppress some of their whispering gallery modes. We investigate the performance of the microring resonator, for various dielectric loss factors between $\tan(\delta) = 0.0001$ and 0.001, and compare the results with a lossless microring resonator.

Since GMT is very close to analytic solutions, it allows experienced users to obtain highly accurate solutions with minimum computational effort. Namely when the boundaries are sufficiently smooth, exponential convergence is reached. Since inexperienced users may create GMT models that are far from being optimal or even fail, GMT is less user-friendly than well-known methods such as FD and FE. Furthermore, it is important to note that exponential convergence is useful for obtaining highly accurate results, whereas methods with slower convergence are usually better suited for obtaining quick results with low or moderate accuracy. As all boundary methods, GMT is much very advantageous for 2D problems because its discretization domain, i.e., the boundaries is only 1D. When extending it to 3D, the discretization domain is squared and therefore, the numerical effort drastically increases. Finally, GMT works with relatively small but dense matrices that tend to be ill-conditioned. Therefore, it is important to implement appropriate matrix solvers. However, the 2D problem considered in the following is well suited to GMT and therefore, highly accurate results are obtained with relatively low numerical effort.

2. ANALYSIS OF A MICRORING USING GMT

GMT can be applied to many computational electromagnetic problems, from static to dynamic, and from scattering to waveguide problems [12]. In dynamic problems, it is based on the expansion of the fields in terms of appropriate basis functions which are solutions to the Helmholtz equation, such as plane waves, multipolar functions, and the modal fields of waveguides. To apply this method to a two-

dimensional (2D) region comprised of multiple domains D_1 to D_n with constitutive parameters ε_n and μ_n, the field in each domain is expanded in terms of analytical solutions of the 2D Helmholtz equations for the corresponding domain. For a TM_z incident field, the only nonzero field components are E_z, H_x, and H_y. The total electric field can be expressed as:

$$E_z^{D_n}(\mathbf{r}) = E_{z,i}^{D_n}(\mathbf{r}) + E_{z,s}^{D_n}(\mathbf{r}) \tag{1}$$

In which $E_z^{D_n}(\mathbf{r})$ is the total electric field in domain D_n, $E_{z,i}^{D_n}(\mathbf{r})$ and $E_{z,s}^{D_n}(\mathbf{r})$ denote the excitation and the scattered electric field in domain D_n, at the observation point $\mathbf{r}$. We can derive other field components (H_x and H_y) in domain D_n, from $E_z^{D_n}(\mathbf{r})$. The coordinate system used here is depicted in Figure 2.

To model the add-drop filter of Figure 1, we use the four-fold symmetry of the structure as shown in Figure 2, which allows us to simulate one quarter of the structure only. We consider a single-

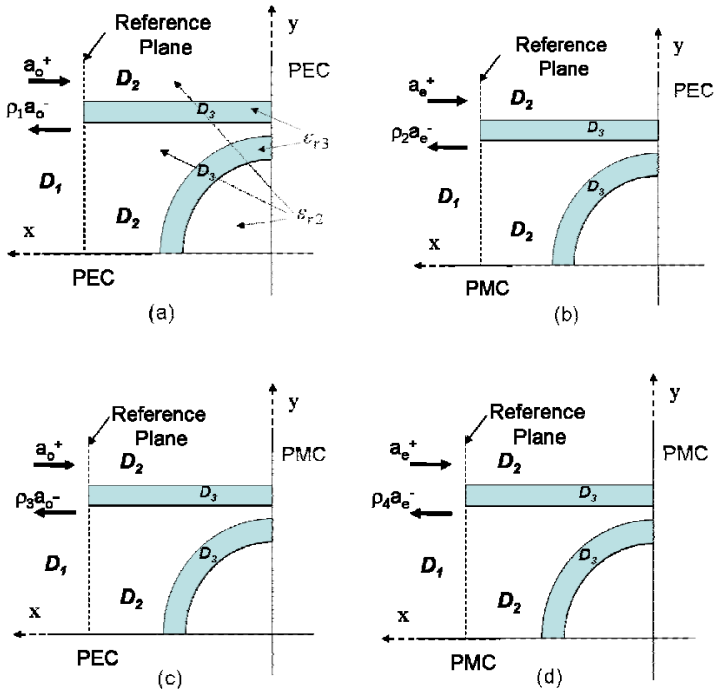

Figure 2. Analysis of a microring add/drop filter using the four-fold symmetry of the structure.

mode waveguide at all of the four waveguide ports. For computing the scattering parameters, we need to define a reference plane (waveguide port) at some distance from the microring. We subdivide each region of Figure 2 into 3 subdomains as shown in the same figure. The field in subdomain D_1 is expanded in terms of the modal fields of two coupled semi-infinite slab waveguides which are attached to the ports P_1 and P_4. Since we use the symmetry of the structure, in D_1 the fields are expanded in terms of the incident and reflected even modes of the coupled waveguides in the configurations depicted in Figures 2(a) and 2(c), and odd modes of the ones shown in Figures 2(b) and 2(d). In domains D_2 andD_3, we expand the total fields using the multipolar functions, so the electric field will be:

$$E_z^{D_{2,3}}(\mathbf{r}) = \sum_{p=1}^{P} \sum_{n=1}^{N_p} \left(A_n \cos n\varphi_p + B_n \sin n\varphi_p\right) H_n^{(2)}\left(k_{2,3}\left|\mathbf{r} - \mathbf{r}_p\right|\right) \quad (2)$$

where the time dependence is assumed as $\exp(j\omega t)$, in which ω is the angular frequency, φ_p represents the azimuth angle at which the field point $\mathbf{r}$ is seen by the p-th multipole located at $\mathbf{r}_p$. P is the total number of multipole clusters, and N_p denotes the maximum order of multipoles in each cluster. Here, $k_{2,3} = \omega\sqrt{\mu_0\varepsilon_0\varepsilon_{r\,2,3}}$, where $\varepsilon_{r\,2,3}$ is the complex relative permittivity of the subdomains D_2 and D_3.

The unknown amplitudes of the reflected wave at D_1, and the coefficients A_n and B_n in (2) are calculated by applying the boundary conditions on the reference plane and the interface of D_2 and D_3, using the generalized point matching technique [12] and QR factorization for the resulting overdetermined system of equations. To take perfect electric conductor (PEC) and perfect magnetic conductor (PMC) boundaries into account, we apply the mirror principle and set the mirror multipoles as in Figure 3. The amplitudes (A_n and B_n) of mirror multipoles have some simple relations with the original ones — dependent on the order of multipoles (n). For every multipole to satisfy the PEC boundary conditions, we have:

a) For a vertical PEC, the amplitudes of the mirror multipoles are multiplied by $(-1)^{n+1}$ for the cosine terms and by $(-1)^n$ for the sine terms of (2), in which n denotes the order of the multipole.
b) For a horizontal PEC, the amplitudes of the mirror multipoles are multiplied by (-1) for the cosine terms and by 1 for the sine terms.

For the PMC boundary conditions, one has similar relations with an additional factor (-1). It should be mentioned that the locations of the multipoles are almost arbitrary, as long as they satisfy some

simple constraints, described in [13]. A typical location for multipoles is shown in Figure 3.

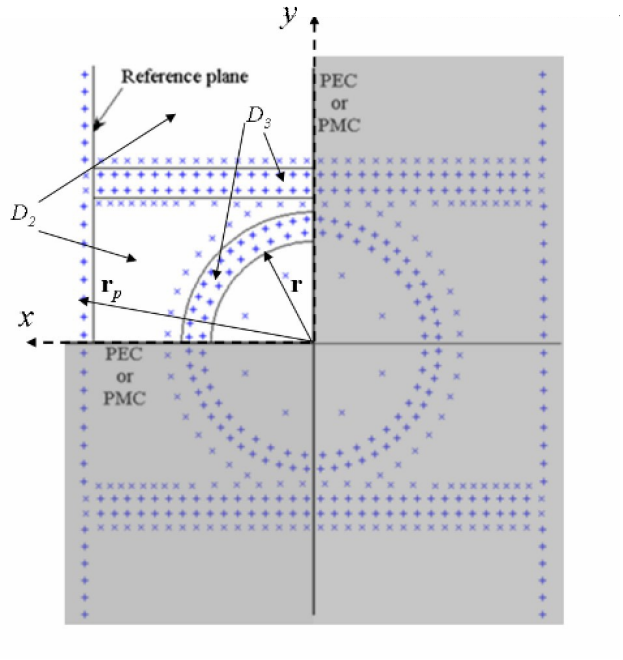

Figure 3. Location of the clusters of multipoles for expanding the fields of domain D_2 is indicated by $+$, and for the fields of domain D_3 is shown with $\times$, the mirror multipoles are located in the shaded region, and their amplitudes are given by the described rules.

If we consider the microring structure as a 4-port circuit, then due to its isotropy and symmetry, the scattering matrix should be as follows:

$$[S] = \begin{bmatrix} S_{11} & S_{21} & S_{31} & S_{41} \\ S_{21} & S_{11} & S_{41} & S_{31} \\ S_{31} & S_{41} & S_{11} & S_{21} \\ S_{41} & S_{31} & S_{21} & S_{11} \end{bmatrix} \tag{3}$$

Note that it is sufficient to calculate the four values S_{11}, S_{21}, S_{31}, and S_{41}. because of the four-fold symmetry of the structure, the scattering parameters can be calculated from the reflection coefficient (ρ_i) obtained from the analysis of the structures shown in Figure 2,

and can be written as:

$$\begin{aligned} S_{11} &= \frac{1}{4}(\rho_1 + \rho_2 + \rho_3 + \rho_4) \\ S_{21} &= \frac{1}{4}(-\rho_1 - \rho_2 + \rho_3 + \rho_4) \\ S_{31} &= \frac{1}{4}(\rho_1 - \rho_2 - \rho_3 + \rho_4) \\ S_{41} &= \frac{1}{4}(-\rho_1 + \rho_2 - \rho_3 + \rho_4) \end{aligned} \tag{4}$$

in which ρ_i is the reflection coefficient of the first modal field of the slab waveguide in the i-th configuration shown in Figure 2.

3. NUMERICAL RESULTS

Using the method described above, we calculate the scattering parameters of an add/drop filter, with $W = 0.2\,\mu$m, $r_i = 1.6\,\mu$m, $r_o = 1.8\,\mu$m, $g = 0.2\,\mu$m, $\varepsilon_{r\,2} = 1$, and $\varepsilon_{r\,3} = 9$. The total number of multipoles in the domains D_2 and D_3 was 1161, and the size of the resulted overdetermined matrix was 3420×1161, because the number of matching points in the generalized point matching technique was 3420. The locations of multipoles are shown in Figure 3. For this number of multipoles the largest relative mismatching error along the boundaries

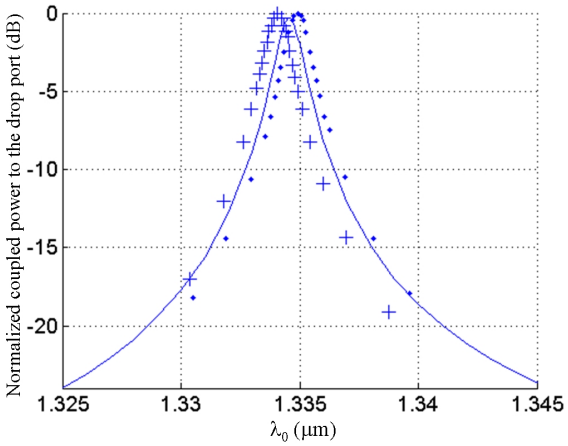

Figure 4. Comparison of GMT (solid curve), CMT (plus signs, [6]) and FDTD (dots, [6]) for the normalized power coupled to the drop port of a microring add/drop filter.

is only 0.1%. To verify the results, we compare the normalized coupled power to the drop port, i.e., $|S_{41}|^2$ with the ones computed in [6] using FDTD and CMT methods. The results are shown in Figure 4. It can be seen that the exact location of the resonance is slightly different for these 3 methods. In the CMT method of [6], the radiation loss has not been taken into account, and the amplitude of the coupled power at the drop port at resonance is computed to be unity. However, exact analysis of this structure using GMT shows a nonzero *IL*. It means that there is a radiation loss due to the diffraction at the ring resonator. The GMT results are more accurate than FDTD results, because of its low error on the boundary (where usually much higher errors are observed than elsewhere), its exponential convergence and the other advantages mentioned above. Compared with CMT, the GMT results must be more accurate because GMT takes the radiation losses into account. In Figure 5, the computed value of FSR for the modes $m = 18$ and 19, where m denotes the number of wavelengths along the perimeter of the ring, is 56 nm. This corresponds to 9.0473 GHz which is comparable to the rough estimation of the following equation which treats the ring resonator as an average radius of $r = 1.7\,\mu$m:

$$FSR = \frac{c}{2\pi n r} = 9.355\,\text{GHz} \tag{5}$$

in which c is the velocity of light in free space and n is the refractive index of the ring resonator.

The quality factor of the ring resonator is obtained as the ratio of the centre frequency to the half power resonance width. Its values along with the centre frequencies for the successive resonances of Figure 5 are listed in Table 1. It can be seen that by increasing the wavelength, the quality factor decreases. This is because the quality factor varies as a function of coupling coefficient (κ) according to:

$$Q \approx \frac{2\pi^2 r\, n_{eff}}{\lambda_0 \kappa^2} \tag{6}$$

Table 1. Resonance data from Figure 5.

Resonance modes (m)	Resonance wavelength (nm)	Half power resonance width (nm)	Quality factor
18	1390.60	1.85	752.34
19	1334.56	1.26	1054.46

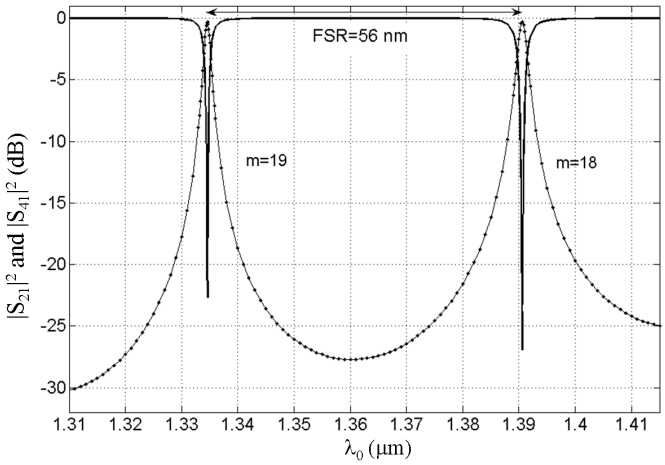

Figure 5. Scattering parameters of $|S_{21}|^2$ (solid line) and $|S_{41}|^2$ (dotted line) for two successive resonance modes of 18th and 19th for a microring resonator with $W = g = 0.2\,\mu$m, $r_i = 1.6\,\mu$m and $r_o = 1.8\,\mu$m.

which is obtained from the CMT [6]. Where $r = 0.5(r_i + r_o)$, n_{eff} is the effective index number of the ring and λ_0 is the wavelength in free space. Since κ increases by increasing the wavelength as described in [7], Q inversely changes with the wavelength.

The insertion loss (IL) is defined as the normalized output power level at the drop port at the resonance wavelength. Its value for the 18th resonance mode ($\lambda_0 = 1390.6\,$nm) in Figure 5 is $-0.296\,$dB. The crosstalk (XL) is the difference between the powers coupled to ports 2 and 4 from port 1 in the vicinity of the resonance. Its value at the same wavelength is 26.6 dB which is assumed as a good crosstalk level. Figure 6 shows the computed electric field at $t = 0$ for the 18th resonance mode.

In the following, we illustrate the effect of the dielectric loss on the transmittance behavior of the ring resonator add-drop filter. Neglecting the surface roughness of the rings, there are two loss mechanisms that affect Q and IL of an ideal ring resonator, namely radiation loss and material loss. For a lossless structure, the ratio of the radiation loss to input power is given by the normalized power loss:

$$\frac{P_r}{P_{in}} = 1 - |S_{11}|^2 - |S_{21}|^2 - |S_{31}|^2 - |S_{41}|^2 \tag{7}$$

When the materials (dielectric substrate, the etched waveguides,

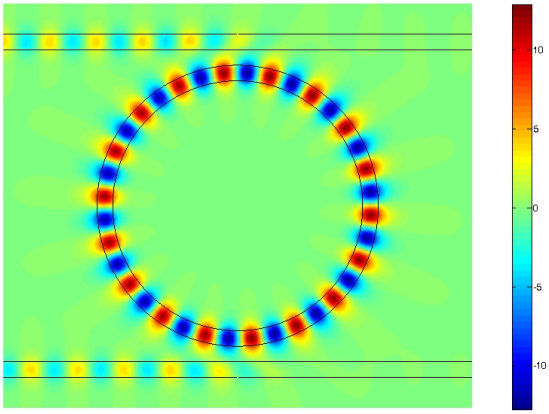

Figure 6. Computed electric field at $t = 0$ and $\lambda_0 = 1.3906$ using GMT method.

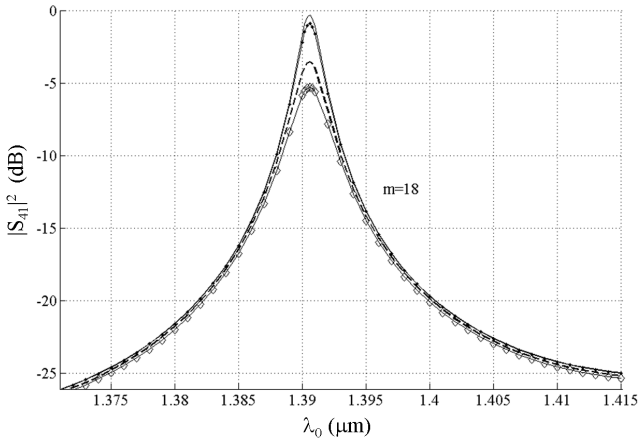

Figure 7. Comparison between different loss factors for the computed coupled power at the drop port: for $\tan(\delta) = 0$ (solid line), $\tan(\delta) = 0.0001$ (dotted line), $\tan(\delta) = 0.0006$ (dashed line), and $\tan(\delta) = 0.001$ (diamond-line).

and the ring) are lossy, the right term in (7) gives the total amount of loss including radiation loss and dissipated power due to the dielectric losses.

Figure 7 shows the normalized coupled power to the drop port for lossless and lossy dielectrics of domain D_2, obtained from (7). From

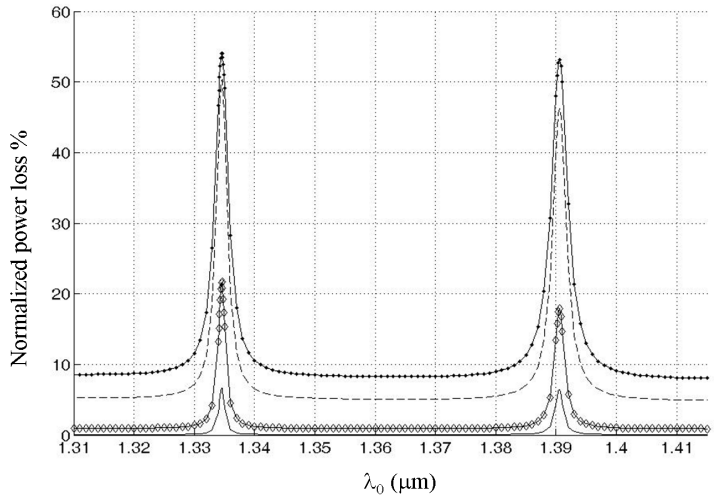

Figure 8. Normalized power loss (Equation (7)) for $\tan(\delta) = 0$ (solid line), $\tan(\delta) = 0.0001$ (diamond-line), $\tan(\delta) = 0.0006$ (dashed line), and $\tan(\delta) = 0.001$ (dotted line).

this, one can see how the dielectric loss factor ($\tan(\delta)$) affects the *IL* of the structure. *Q* and *IL* for various dielectric loss factors are shown in Table 2. In Figure 8, the normalized power losses for the mentioned loss factors are shown. It can be seen that highest losses are obtained at resonance wavelengths. That is because of the bending loss which is much higher at resonances due to high coupling of fields in the ring at those wavelengths. It is apparent from Table 2 that the *IL* for the 18th resonance mode is higher than the one for the 19th resonance mode. This is because of the higher coupling efficiency for the resonance mode $m = 18$ due to higher resonance wavelength. Also for lossy dielectrics, the IL deteriorates more rapidly by increasing the dielectric loss factor for the 19th resonance mode in comparison with the $m = 18$ case, which leads also to a higher decrease in the quality factor of the resonance mode $m = 19$.

The total amount of power loss changes nonlinearly at the resonance wavelength. It is apparent from Figure 8 that the power loss at the resonance wavelengths for $\tan(\delta) = 0.001$ is slightly higher than the 50% of the incident power, and this is nearly the case for both resonances, but for lower dielectric loss factors, the amount of dissipated power is different for these resonances, and for $\tan(\delta) = 0$, they are again nearly the same.

Table 2. Quality factor (Q) and insertion loss (IL) for couplers with lossy dielectrics.

Dielectric loss factor	Resonance mode number (m)	Insertion loss (dB)	Quality factor
0	19	−0.325	1054.46
	18	−0.296	752.34
0.0001	19	−1.158	942.82
	18	−0.908	707.97
0.0006	19	−4.593	667.52
	18	−3.565	533.15
0.001	19	−6.704	529.33
	18	−5.300	439.59

4. CONCLUSION

The scattering parameters of a ring coupler with lossy dielectric were efficiently and accurately computed with the generalized multipole technique after taking the four-fold symmetry of the structure into account for reducing the computational effort. The results were validated by comparisons with CMT and FDTD results — that are in fact less accurate than our GMT results. It is important to note that GMT allows us to take the dielectric losses as well as radiation losses into account without any numerical problems. The Q and IL of the microring resonator for different dielectric loss factors were computed for two successive modes of the ring coupler, and we showed that IL varies differently for these modes. The total normalized power loss has been computed using the obtained scattering parameters and the behavior of the total loss at resonance wavelengths have been shown to change nonlinearly with the dielectric loss factor.

ACKNOWLEDGMENT

The authors would like to thank Iran Telecommunications Research Centre (ITRC) for their support of this project.

REFERENCES

1. Bozhevolnyi, S., V. Vokov, E. Devaux, J. Laluet, and T. Ebbesen, *Nature Lett.*, Vol. 440, 508–511, 2006.
2. Schwelb, O., *Elsevier Opts. Comms.*, Vol. 265, 175–179, 2006.
3. Madsen, C. and G. Lenz, *IEEE Photonics Technol. Lett.*, Vol. 10, 994–996, 1998.
4. Little, B., S. Chu, W. Pan, and Y. Kokubun, *IEEE Photonics Technol. Lett.*, Vol. 12, 323–325, 2000.
5. Krauss, T. and P. Laybourn, *Proc. SPIE*, Vol. 1583, 150, 1994.
6. Little, B., S. Chu, H. Haus, J. Foresi, and J. Laine, *J. Lightwave Technol.*, Vol. 15, 998–1005, 1997.
7. Hagness, C., T. Rafizadeh, T. Ho, and A. Taflove, *J. Lightwave Technol.,* Vol. 15, 2154–2165, 1997.
8. Yuan, W. and E.-P. Li, *Progress In Electromagnetics Research*, PIER 47, 193–212, 2004.
9. Ziolkowski, R. W., *Progress In Electromagnetics Research*, PIER 41, 159–183, 2003.
10. Moreno, E., D. Erni, and C. Hafner, *Phys. Rev. E*, Vol. 66, 036618(10), 2002.
11. Moreno, E., D. Erni, and C. Hafner, *Phys. Rev. B*, Vol. 65, 155120(10), 2002.
12. Hafner, C., *The Generalized Multipole Technique for Computational Electromagnetics*, Artech House, Boston, 1990.
13. Moreno, E., E. Erni, C. Hafner, and R. Vahldieck, *Opt. Soc. Am. A*, Vol. 19, 101–111, 2002.